

First-principles study of electronic structure and charge transport at PTCDA molecular layers on Ag(111) and Al(111) electrodes

Tatsuhiko Ohto,¹ Koichi Yamashita,¹ and Hisao Nakamura^{2,*}

¹*Department of Chemical System Engineering, Graduate School of Engineering, the University of Tokyo, Tokyo 113-8656, Japan*

²*Nanosystem Research Institute (NRI), "RICS," Advanced Industrial Science and Technology (AIST), Central 2, Umezono 1-1-1, Tsukuba, Ibaraki 305-8568 Japan*

(Received 10 June 2010; revised manuscript received 29 November 2010; published 8 July 2011)

We performed first-principles transport calculations of the contact consisting of 3,4,9,10-perylenetetracarboxylic dianhydride (PTCDA) molecular layers and metal electrodes using the nonequilibrium Green's function method combined with the density functional theory. To analyze roles of organic/metal interfacial states for transport, we examined two kinds of electrodes: Ag(111) and Al(111). By quantitative evaluation of the coupling strength between PTCDA molecular orbitals and electrodes, we found the creation of the Shockley-type state at the interface of PTCDA and Ag(111). In contrast, the Al(111) surface formed a strong chemical bond with PTCDA. A clear Shockley-type state was not created, and an ohmic bias voltage (V) and electric current (I) behavior was found for contacts consisting of thin PTCDA layers and Al(111) electrodes. We also predicted that further stacking of PTCDA layers will make I - V characteristics more Schottky-like for both Ag and Al electrodes, regardless the different microscopic mechanism.

DOI: [10.1103/PhysRevB.84.045417](https://doi.org/10.1103/PhysRevB.84.045417)

PACS number(s): 73.23.Ad, 73.20.At

I. INTRODUCTION

The understanding of charge transport at interfaces is important for its potential applications in organic-based devices, as well as for its fundamental aspects, because organic devices often have layered structures and carriers pass through the interfaces.¹⁻⁵ The alignment of molecular levels with respect to the Fermi level of the metal is the factor responsible for the mechanism of charge injection at the interface.^{6,7} Because of the formation of the interfacial dipole, the barrier height for charge injection at the interface is dramatically different from that predicted by the simple Schottky-Mott model.^{6,7} The mechanism of formation of the interfacial dipole largely depends on the electronic states of both the organic materials and the metal surfaces. Therefore, many experimental⁸⁻¹² and theoretical¹³⁻²¹ studies have investigated the structural and electronic properties of adsorbed molecules on metal surfaces, similar to adsorption-induced changes of work functions.²²⁻²⁵

The metal surface system covered with 3,4,9,10-perylenetetracarboxylic dianhydride (PTCDA) is one of the most studied organic/metal interfaces.²⁶⁻³⁶ The molecular crystal of PTCDA (α, β) can be regarded as a stack of molecular (102) planes.^{37,38} The difference between α and β phases is that the stacking axis is tilted in the direction of the long (α) or the short (β) axis of the (102) cell. Because of the planarity, PTCDA tends to grow as a highly ordered film on many metal surfaces.³⁹⁻⁴¹ On the Ag(111) surface in particular, a commensurate layer of PTCDA is formed by the moderate interaction between PTCDA and Ag, up to two monolayers (2 ML).⁴²⁻⁴⁶ An interface between PTCDA monolayer and Ag(111) is free from disorder. Hence, this system has been actively investigated to identify the intrinsic electronic properties of molecular semiconductors at the interface.⁴⁷⁻⁵⁹ The most notable features of PTCDA overlayers on Ag(111) are their exotic interfacial states. The lowest unoccupied molecular orbital (LUMO) of PTCDA is partially occupied by an electron from the Ag(111) surface, and the occupancy

of this interfacial state decreases with increasing coverage.⁵⁷ The PTCDA layer forms a Shockley-type interfacial state on Ag(111).⁵⁰ LUMO+1 and LUMO+2 of PTCDA molecules are mixed with the Shockley state of the Ag(111) surface and strongly disperse in two dimensions. Such an interfacial state may affect the transport properties at the interface. Recently, Schwab *et al.* suggested that these interfacial states should be included in theories of level alignment and barrier formation at organic/metal interfaces.⁶⁰

However, even as the electronic states have been debated and investigated, scarce attention has been devoted to the transport properties of PTCDA and the role of metal electrodes from the microscopic point of view. To evaluate the role of the interfacial state, comparison with Ag(111) and Al(111) will be useful because of the absence of the Shockley state in Al(111).^{61,62} Several studies reported the macroscopic characteristics of bias voltage (V) and electric current (I), which are called I - V characteristics, of both interfaces. Hirose *et al.* measured I - V characteristics for interfaces between several metals and PTCDA layers 1800 Å thick, suggesting that nonreactive metals (i.e., Au, Ag, and Cu) show Schottky-type behavior ($I \propto \exp(V)$), whereas reactive metals (Al and Ti) show ohmic behavior ($I \propto V$).⁶³ This ohmic behavior is attributed to the gap states caused by metal oxides. Agrawal and Ghosh also measured the electric current of 100- to 400-nm PTCDA layers with Al electrodes and obtained a Schottky-type I - V behavior rather than an ohmic behavior.⁶⁴

In this work, we investigated the transport properties of the contact of PTCDA and Ag and Al electrodes, which are denoted as Ag(111)/PTCDA/Ag(111) and Al(111)/PTCDA/Al(111), respectively. Estimation of I - V characteristics were carried out by the nonequilibrium Green's function (NEGF) formalism combined with density functional theory (DFT). To apply NEGF-DFT, we introduced the periodic molecule structure for contacts as a model of the (experimentally observed) commensurate layer structure to

reduce computational cost. We denote this model as the periodic molecular model, where PTCDA overlayers are stacked as dimers or trimers because of restricted periodicity. However, lateral interactions between neighbor molecules are included in this model. To check the validity of the preceding simplification and the accuracy of adopted computational methods, we carried out several preliminary calculations of PTCDA overlayers on (single-side) metal substrate using a standard slab approach. These calculations are denoted as PTCDA/metal contacts and named the surface-slab model, because surface-slab systems are easy to compare with previous theoretical and experimental studies. We focus on whether very thin PTCDA film in contact shows clear Schottky-type or ohmic behavior, examining the dependence on kinds of metal and the number of molecular layers. The role of the interfacial state is discussed from the view of molecular orbitals (MOs) based on resulting Green's functions.

This paper is organized as follows. In Sec. II, we describe the computational scheme and show calculated results of the PTCDA layer adsorbed on Ag(111) or Al(111) substrate (surface-slab model) using a standard slab approach. Analysis of electronic structures at interfaces and conformation of stacking of PTCDA layers and/or lateral interactions are shown. Several models of a (surface) unit cell are also discussed. We set up model structures of the contacts Ag/PTCDA/Ag and Al/PTCDA/Al for transport calculations in Sec. III. We then describe the details of transport properties, effects of stacks of PTCDA layers, and PTCDA-metal interactions in Sec. IV. A summary and conclusions are presented in Sec. V.

II. COMPUTATIONAL METHOD AND ELECTRONIC STRUCTURE AT THE PTCDA/METAL INTERFACE

A. Computational method

DFT,⁶⁵ as implemented in the SIESTA package,⁶⁶ was employed for the calculation of the electronic structure. We used a single- ζ polarized basis set for metal atoms and a double- ζ polarized basis set for H, C, and O atoms. Core electrons are described by the Troullier-Martins norm-conserving pseudopotential⁶⁷ with the Kleinman-Bylander nonlocal projector.⁶⁸ We used the local density approximation (LDA) functional, although LDA sometimes overestimates bonding strengths and cannot estimate the long-range force correctly. The validity of using LDA is briefly described later. We examined $p(6 \times 7)$, $p(4 \times 6)$, and $(\frac{7}{2} \frac{1}{5})$ fcc (111) unit cells to impose two-dimensional periodicity of the surface; these represent the adsorbed structures of PTCDA as a single molecular structure, periodic molecular structure, and commensurate layer, respectively. The Brillouin zones of all cells were sampled with Monkhorst-Pack⁶⁹ $2 \times 2 \times 1$ k-grids. We optimized each structure by relaxing only atoms of PTCDA. Before setting up contacts (i.e., Ag/PTCDA/Ag and Al/PTCDA/Al) for NEGF-DFT, we performed preliminary calculations for surface-slab (PTCDA/Ag and PTCDA/Al) systems. They are used to check the validity of our computational schemes and for complementary analyses of interfacial states.

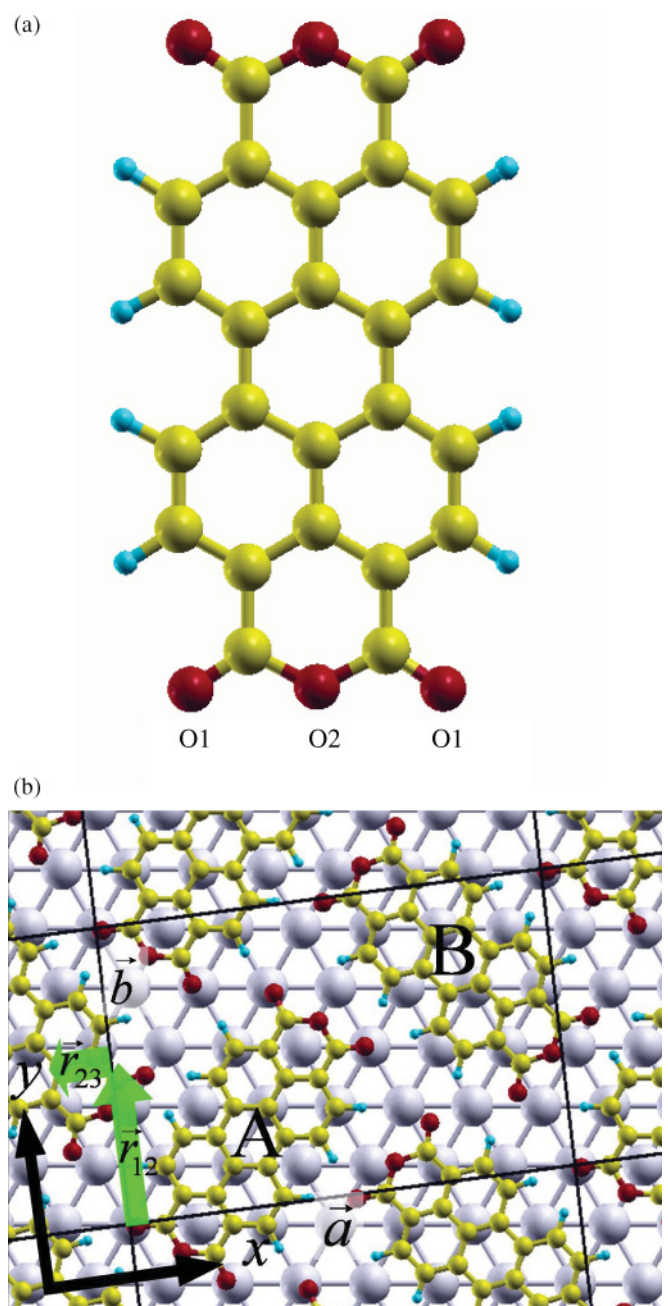


FIG. 1. (Color online) (a) Schematic view of a PTCDA molecule. O1 is a carboxyl O atom, and O2 is an anhydride O atom. (b) Commensurate PTCDA layer over an Ag(111) surface. Yellow (light gray), light blue (dark gray), red (black), and large silver (white) balls mean C, H, O, and Ag, respectively. In (b) \vec{a} is the long axis and \vec{b} is the short axis of the unit cell; \vec{r} shows the lateral displacement of the next PTCDA layer; and A and B show different kinds of PTCDA molecules in the unit cell of the commensurate layer structure.

B. Preliminary calculations: Single-monolayer PTCDA on Ag and Al substrates

Before constructing contact models for transport calculations, we calculated 1-ML PTCDA on a single-side metal substrate. First, we show DFT results of the commensurate layer structure of PTCDA/Ag(111) in the surface-slab approach. Figures 1(a) and 1(b) show a schematic view of the

TABLE I. Adsorption structures of the models (single and periodic molecular models and commensurate layer) for monolayer PTCDA on the Ag and/or Al substrate. The labels C, O1, and O2 for atoms and the notation of the types A and B are summarized in Fig. 1. The letter M represents the metal atom (Ag or Al) nearest each C, O1, and O2 atom, and the averaged distance between atom X and atom M is denoted as X -M in the table. In the rightmost column, $\Delta\Phi$ represents the change in work function from that of the clean metal.

Metal substrate	Structure (model)	C-M (\AA)	O1-M (\AA)	O2-M (\AA)	$\Delta\Phi$ (eV)
Ag(111)	single molecule	2.91	2.44	2.73	-0.07
	periodic molecule	2.82	2.42	2.71	-0.21
	type A (commensurate layer)	2.75	2.50	2.77	-0.20
	type B (commensurate layer)	2.72	2.59	2.78	-0.20
	exp ⁴⁰	2.86	2.68	2.97	0.27 ⁵⁵ , -0.10 ⁴⁰
Al(111)	periodic molecule	2.89	1.97	2.55	-0.12

PTCDA molecule and top view of the 1-ML PTCDA/Ag(111), respectively. The surface plane of PTCDA/Ag(111) is the x - y plane, and the x axis is set to the long axis, \vec{a} . The z axis is perpendicular to the x - y plane. As we stated in the introduction, the adsorption structures of a single PTCDA and a commensurate PTCDA monolayer on the Ag(111) surface have been studied thoroughly.²⁶ The carbon framework of the single PTCDA is almost flat, whereas the carboxylic O atoms approach the Ag atoms beneath.²⁶ There are two types of PTCDA molecules in the unit cell of the commensurate layer structure, type A and type B (Fig. 1(b)). The lateral position of the former is similar to that of the single PTCDA. The carboxylic O-Ag distances of the latter are slightly larger than those of the former, because O atoms do not lie on atop sites of the Ag(111). Our calculated results reproduced the previous experimental⁴⁰ and computational⁵⁹ works, as shown in Table I.

Figure 2(a) shows the density of states projected onto the PTCDA molecules of commensurate layers (the curve labeled 1 ML). The partially occupied LUMO and the strongly dispersed LUMO+1 are properly described. The mechanism of the chemical bonding of PTCDA/Ag(111) through the O-Ag bond and charge injection from the substrate to LUMO of PTCDA, i.e., a kind of donation and back donation, is widely accepted.²⁶ LUMO+1 is considered as a part of the Shockley-type interfacial state of PTCDA/Ag(111).²⁶ The energy of the Shockley state of the clean Ag(111) surface is 0.29 eV above the Fermi level at the Γ point, and we found a related state 0.82 eV above the Fermi level in the present commensurate layer structure. In the region on PTCDA, wave function of this state is similar to that of LUMO+1 of a free PTCDA molecule, and the value 0.82 eV is in good agreement with the experimental observation for the interfacial state.⁷⁰ Hence, our calculation confirmed that the Shockley-type interfacial state is formed by the hybridization of PTCDA (LUMO+1) and Ag(111) states.

Similar procedures were applied in the case of Al(111). At variance with previous theoretical calculations,⁷¹ the PTCDA molecule largely bends because of the strong O-Al bonding, as shown in Table I. Because the calculation using the Perdew-Burke-Ernzerhof (PBE) functional gives the same result (being the bending even emphasized), we consider that the strong O-Al bonding is a characteristic feature of the interface between PTCDA and Al(111) surface. In addition,

the most stable position of PTCDA on the Al(111) surface is the same as on the Ag(111) surface, i.e., all carboxylic O atoms reside on the top of metal atoms. The projected density of states (PDOS) of the PTCDA molecule is shown in Fig. 2(b). The energy level alignment of MOs against the Fermi level is deeper than that of PTCDA/Ag(111), revealing strong donation and back donation. However, other features,

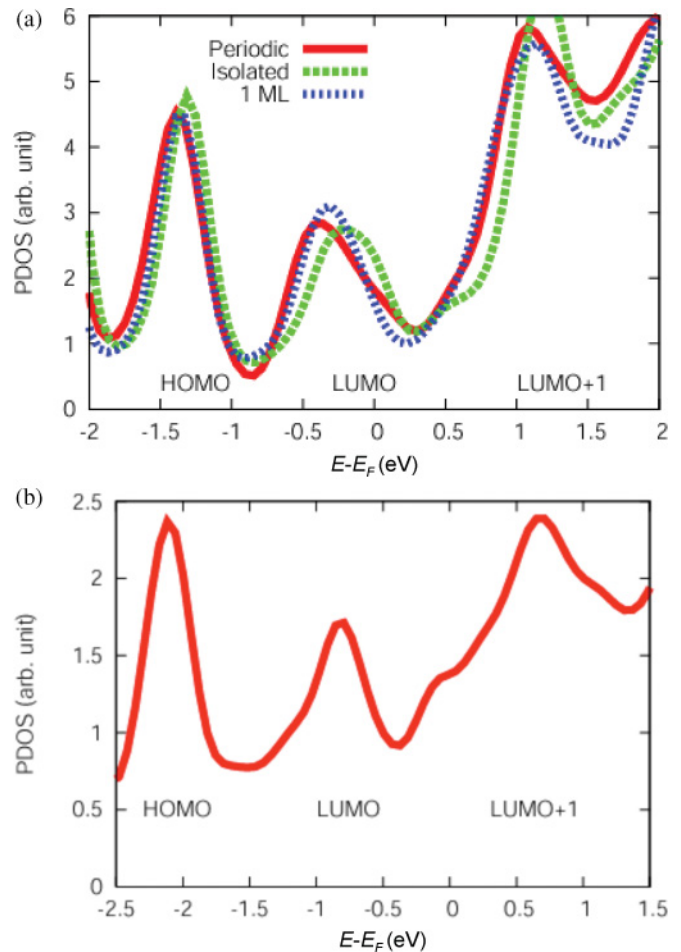


FIG. 2. (Color online) (a) Density of states projected onto PTCDA molecules of the PTCDA/Ag(111) surface-slab model. (b) Density of states projected onto the PTCDA molecule of PTCDA/Al(111) for the periodic molecular structure.

such as the intervals and overall shapes of MOs, are similar between Ag and Al substrates. From the preceding estimation of the energy level alignment, LUMO and LUMO+1 could contribute to transport, i.e., conducting MOs, as in the case of Ag substrate. Furthermore, LUMO+1 is expected to be more conducting, because there is no projected gap.

For later use, we analyzed results of the other two model structures. One is the periodic molecular structure, which is a slightly simplified periodic structure compared to the commensurate layer, as stated earlier. The other is the single molecular structure, where the interactions between neighboring PTCDA molecules are negligible. PDOS of PTCDA is also given for these two models in Fig. 2(a). PDOS of the periodic molecular structure agrees with that of the commensurate layer. The detailed calculations of the (optimized) adsorption structure and work function of the PTCDA overlayer are listed for each model in Table I. Agreement of the PTCDA structures of the periodic molecular model with type A in the commensurate layer structure (Fig. 1(b)) is satisfactory. Furthermore, work functions of these models agree well. Hence, effects of change of the lateral interactions caused by the difference between the periodic molecular and the commensurate layer structures may be negligible for electronic states at the interface.

Consider our use of LDA in the present DFT calculations. Several groups reported that the adsorption structure of PTCDA is reproduced well by some functionals associated with LDA.^{28,41,58,72,73} Because the generalized gradient approximation (GGA) level functional, such as the PBE functional,⁷⁴ sometimes gives an unreasonable adsorption structure and underestimates its energy,⁷⁵ the use of LDA is justified only as the empirical reason. Therefore, we checked the necessity of the van der Waals (vdW) correction for the present study. We confirmed that the vdW correction does not improve the transport property systematically, using several initial test calculations for the PTCDA molecular crystal, as well as the metal interface. The GGA(PBE) overestimated the volume of the crystal by 20%. Although the vdW (Dion-Rydberg-Schroder-Langreth-Lundqvist^{76,77}) correction improved the volume of $\sim 5\%$ with respect to the LDA-calculated volume, the improvement of the band gap is only 0.03 eV. Furthermore, the gap of the highest occupied molecular orbital (HOMO) and the LUMO relating to the PTCDA molecule connected to the metal clusters are almost the same (difference < 0.1 eV) in the case of LDA and vdW correction functionals. Finally, although many-body effects such as GW corrections would be important for quantitative estimation of conductance, practical applications of the first-principles transport calculation are quite limited.^{78–80} All these reasons motivated our decision to use the LDA functional in the calculations.

C. Preliminary calculations: Multilayer PTCDA stacked on the Ag substrate

One of our interests is the change of the electronic structure and of the transport property by the increase in thickness of molecular layers. Unfortunately, the stacking direction of PTCDA possibly differs according to the number of layers or metal species of substrates. If the use of common stacking directions is a good approximation for electronic structure

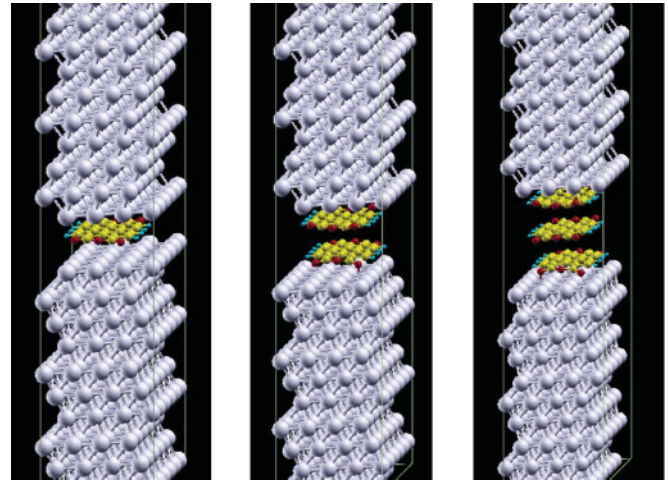


FIG. 3. (Color online) Schematic view of the metal/PTCDA/metal contact of one (1L: left panel), two (2L: middle panel) and three (3L: right panel) layers of PTCDA. Each atom (ball) is represented by the same coloring (shading) as in Fig. 1.

calculations of stacking two or more PTCDA layers, it is useful not only for simplifying the system but also for making comparison between different electrodes. Therefore, we calculated the surface-slab of commensurate layers on Ag(111) up to three monolayers (i.e., 2-ML and 3-ML PTCDA/Ag) just as a reference. After that, we calculated the dimerlike stacking structure of the periodic molecular model and then examined the approximation by using common stacking directions.

The most stable stacking direction of the second layer, \vec{r}_{12} , is (0.11, 6.30, 3.03) Å. This is half of the short axis and is energetically the most stable. The stacking direction of the third layer, \vec{r}_{23} , is (−1.63, −0.02, 3.06) Å, which has a slightly smaller x value than that of the α -crystal: (−1.90, 0.00, 3.22) Å.³⁸ The stacking vectors \vec{r}_{12} and \vec{r}_{23} are shown in Fig. 1(b). Experimentally, it has been reported that the second layer is commensurate with the Ag(111) substrate, displaced $\sim 50\%$ along the short axis from the first layer. Beyond 2 ML, it has been found that the molecule exhibits a Stranski-Krastanov growth like the α -crystal cluster. Therefore, this result is consistent with the experimental observation.⁴⁵ It also has been reported that the third layer does not form a monolayer commensurate with the Ag(111) substrate and that the short vector of (102) mesh is slightly rotated, by $\pm 2.1^\circ$, with respect to the short vector of the commensurate unit cell of the underlying two layers.⁴⁵ However, we adopt the same unit cell as in the cases of 1 and 2 ML, because the difference in angle between the second and the third layers is almost negligible.

The stacking direction of PTCDA molecules in the periodic molecular PTCDA/Ag(111), (−0.40, 1.64, 3.10) Å, which slightly deviates from that of the β -crystal, (0.00, 1.95, 3.24) Å,³⁸ is different in the x and y directions with \vec{r}_{12} or \vec{r}_{23} of the commensurate layer. However, the z -component, i.e., the space between π - π stacking, is equivalent to the latter. Furthermore, despite the difference in stacking directions, the behavior of electronic structure with molecular layers of different thickness is similar. The energy levels

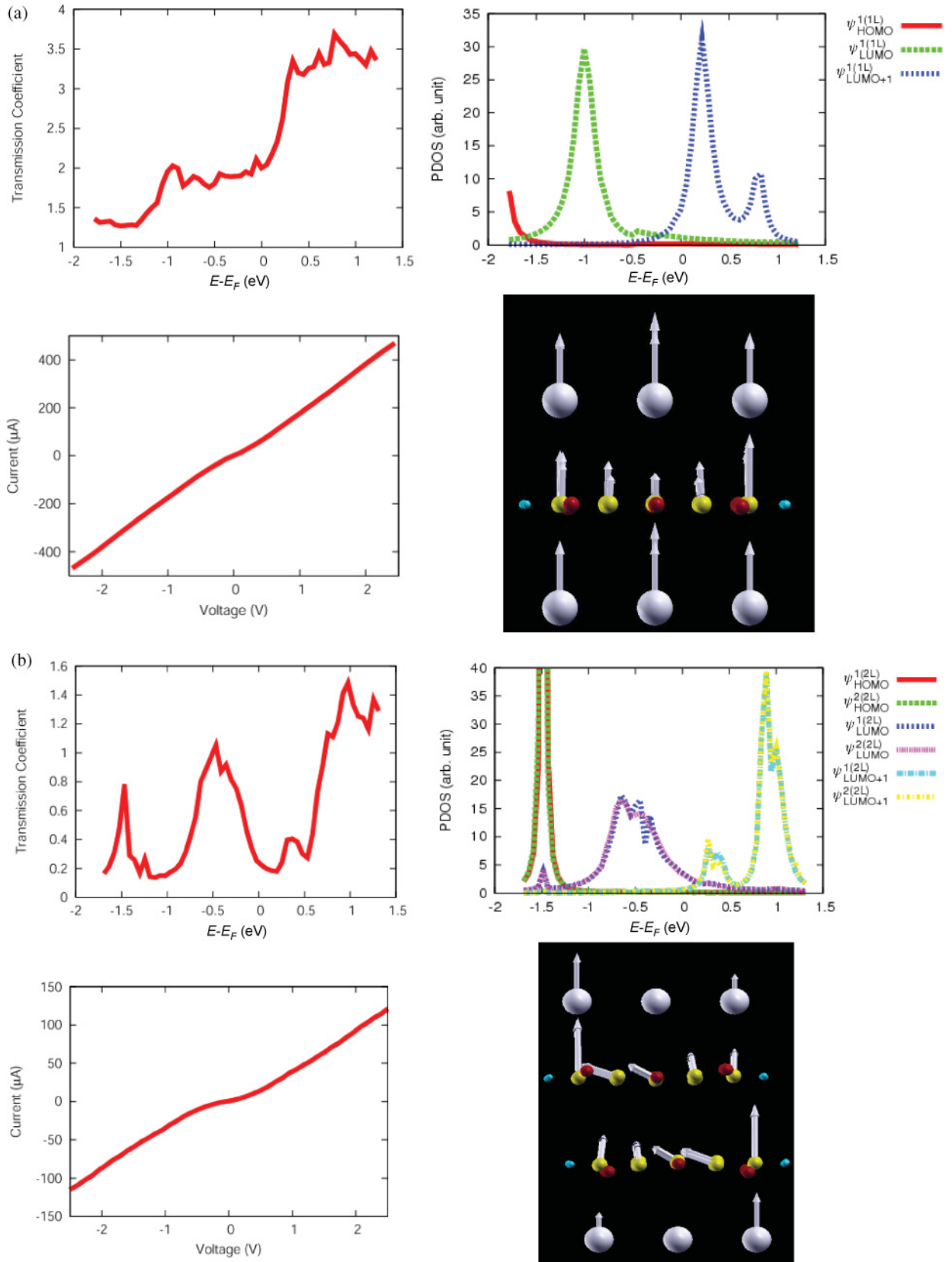


FIG. 4. (Color online) (continued).

of MOs are pulled up because of the increase in thickness without significant split by almost the same degrees for both cases. As a result, we confirm that the periodic molecular

structure reproduces the electronic structure of the commensurate layer structure even in the case of the multilayer stacking.

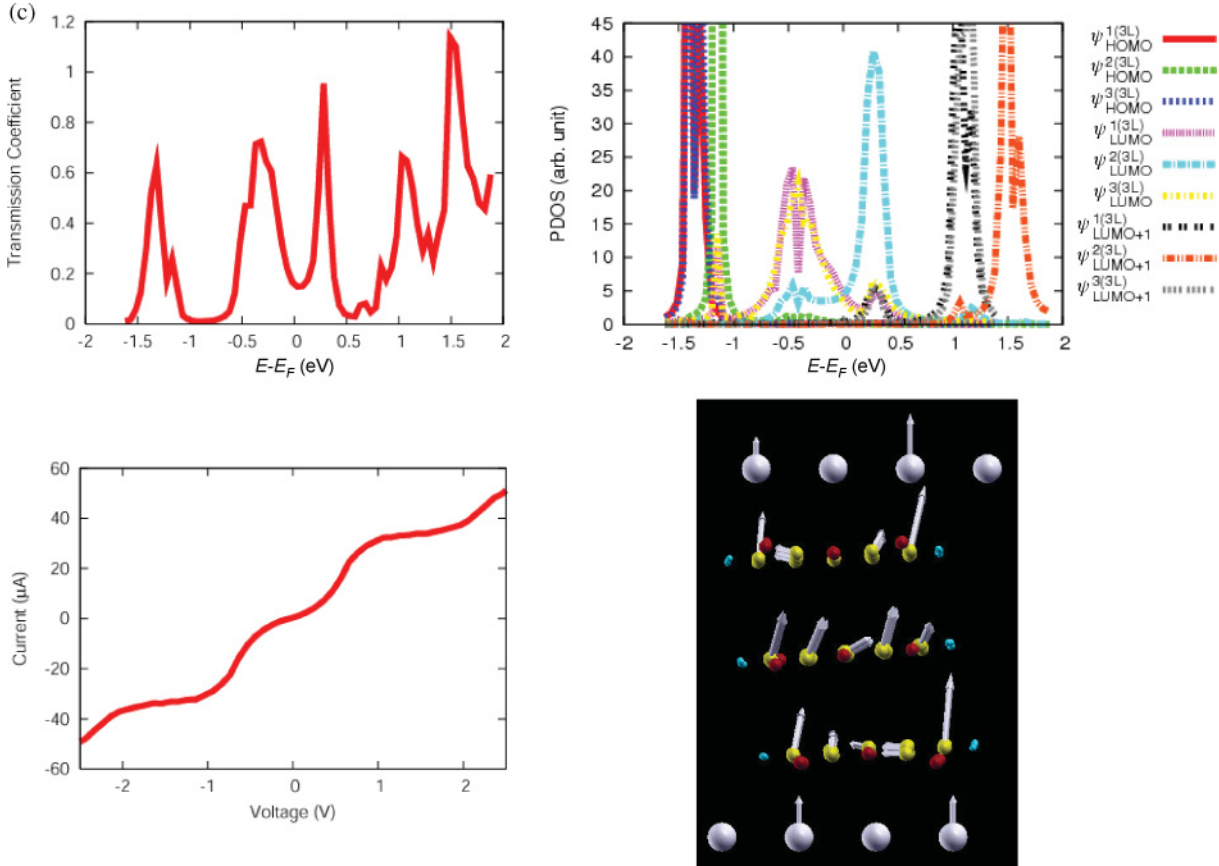


FIG. 4. (Color online) (*continued*). Calculated data set of transport properties for (a) 1L, (b) 2L, and (c) 3L Ag(111)/PTCDA/Ag(111) contacts. The top panels represent the transmission coefficient (left) and density of states of PMOs close to the Fermi level (right). The bottom panels are I - V characteristics (left) and the electron pathway in PTCDA layers (right). Each atom (ball) in the panel of the electron pathway is represented by the same coloring (shading) as in Fig. 1.

III. SETTING UP MODELS OF “CONTACT” FOR TRANSPORT CALCULATIONS

NEGF-DFT is a practical and widely used approach to carry out first-principles transport calculations. However, it is a heavier task computationally than standard DFT, and the system size gets larger than simple surface-slab (PTCDA/metal) because metal substrates are required on the left and right sides (two sides) of the molecular layers (metal/PTCDA/metal). Therefore, applications of NEGF-DFT to the commensurate layer structure are computationally expensive, and a more compact structure is desired to model a contact. Thus, we examine whether simplification by a periodic molecular model is applicable for a modeling contact, as it is in the case of a surface supercell.

The structures of the adopted models are shown in Fig. 3, and we named them the 1L, 2L, and 3L contacts corresponding to the number of stacking layers (1, 2, and 3, respectively). The adsorption site of the PTCDA molecule in contact with the electrode (contact-PTCDA) is the same as that of the type A molecule of the 1-ML PTCDA/Ag(111). On the other hand, the stacking direction of the periodic molecular structure is that of the dimer of PTCDA: $(-0.40, 1.64, 3.10)$ Å. Each PTCDA molecule nearest to each metal surface takes the adsorption structure given in Sec. II, while PTCDA in the middle layer has a planarlike structure, i.e., is close to the structure of a free

molecule or a molecule in a molecular crystal. These results suggest that the periodic molecular model for PTCDA/Ag and Ag/PTCDA/Ag gives a similar structure—at least for PTCDA nearest to electrodes. The periodic molecular structure of PTCDA/Ag was a good approximation of commensurate layers for multilayer PTCDA, as shown in Sec. II C. Hence, we conclude that the use of the periodic molecular model, i.e., the $p(4 \times 6)$ cell, is reasonable to model the contact and to apply NEGF-DFT. A similar check was performed in the case of Al(111). For instance, molecular layers were stacked in the direction of the dimer in the periodic molecular structure on Al, just as in the case of Ag electrodes. The modeling of contact by the periodic molecular structure is also applicable to Al(111) electrodes.

IV. TRANSPORT PROPERTIES

A. Theoretical background

The ballistic current I for the given bias V_b can be written using Green’s function $\mathbf{G}(E)$ in matrix form as

$$\begin{aligned}
 I(V) &= G_0 \int dE \text{Tr}[\Gamma_L(E)\mathbf{G}(E)\Gamma_R(E)\mathbf{G}^\dagger(E)] \\
 &\quad \times (f_L(E) - f_R(E)) \\
 &= G_0 \int dE T(E) (f_L(E) - f_R(E)), \quad (1)
 \end{aligned}$$

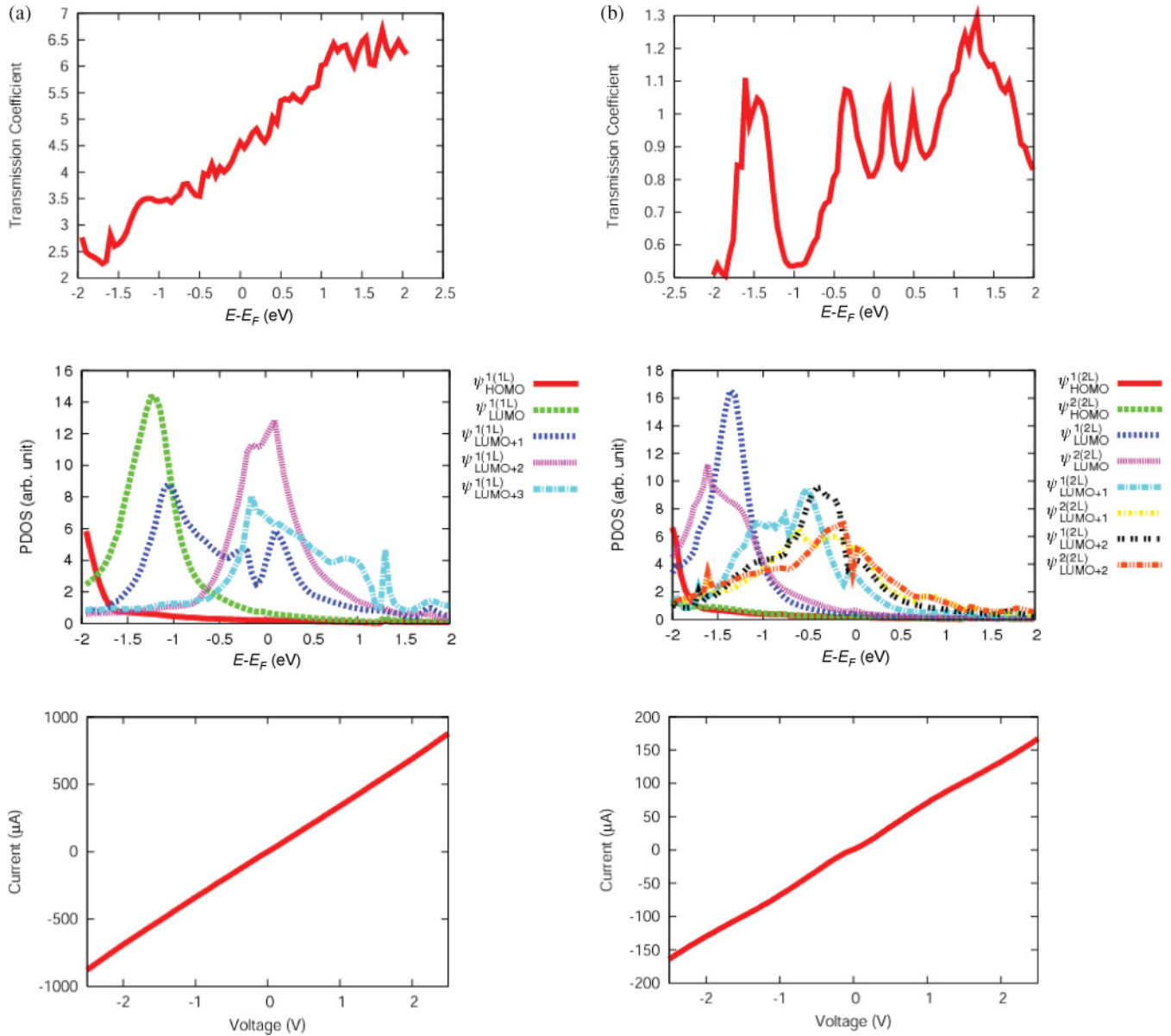


FIG. 5. (Color online) For legend see next page.

where $f_{L/R}$ is the Fermi distribution function with chemical potential $\mu_{L/R}$ of the left (right) leads $L(R)$. E is one-electron energy, and $T(E)$ is a transmission coefficient. $\Gamma_{L/R}$ is defined as $i(\Sigma_{L/R} - \Sigma_{L/R}^\dagger)$, where $\Sigma_{L/R}$ is the lead self-energy. The terms of semi-infinite electrodes are exactly renormalized to the contact region, although the explicit contact consists of nine metal layers of both electrodes and bridge molecules in the NEGF-DFT. To analyze interfacial states and their role to conductance, we calculated the projected molecular orbitals (PMOs), where the PMOs are defined as the eigenstates of the molecular projected state Hamiltonian \mathbf{H}_{mol} .⁸¹ When we expand the renormalized energy term by the PMO basis, we can evaluate the coupling between molecules and outer electrodes. The resulting energy shift and molecule-electrode coupling strength for each PMO, ψ_α , can be

expressed as

$$\begin{aligned} \Delta(\psi_\alpha) &= \text{Re}(E_\alpha^0 - \langle \psi_\alpha | \mathbf{G}^{-1}(E_\alpha^0) | \psi_\alpha \rangle) \\ \gamma(\psi_\alpha) &= -\text{Im}(E_F - \langle \psi_\alpha | \mathbf{G}^{-1}(E_F) | \psi_\alpha \rangle), \end{aligned} \quad (2)$$

where E_F is the Fermi energy at zero bias and E_α^0 is the eigenvalue of \mathbf{H}_{mol} . The Fermi level is set to 0 throughout this paper. Here, α is assumed to be the HOMO or LUMO of the free PTCDA molecule. Therefore, the LUMO is partially occupied by the electron from the electrodes, while the HOMO is far from the Fermi level in the contact systems. We denote the PMO of the mL contact ($m = 1, 2, \text{ or } 3$) as $\psi_\alpha^{n(mL)}$, where the projection is defined on PTCDA in the n th layer far from the left electrode. For instance, $\psi_\alpha^{1(3L)}$

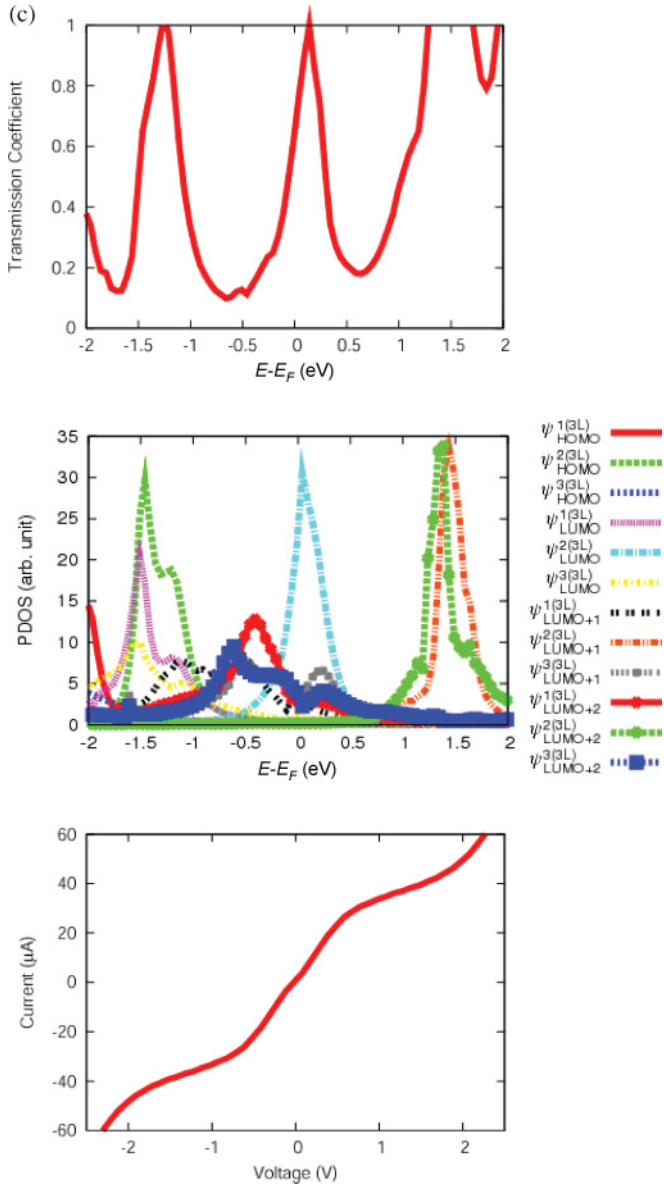


FIG. 5. (Color online) Calculated data set of transport properties for (a) 1L, (b) 2L, and (c) 3L Al(111)/PTCDA/Al(111) contacts. The top panel represents the transmission coefficient, and the middle panel is the density of states of PMOs close to the Fermi level. The bottom panel is the I - V curve.

and $\psi_{\alpha}^{3(3L)}$ correspond to the PMOs of PTCDA molecules interfaced with the left and the right electrodes, respectively.

Furthermore, the nonequilibrium electron pathway from atom A can be defined by the local current vector, using Green's function, as

$$\vec{J}_A = G_0 V \sum_{B \neq A} \vec{u}_{AB} \sum_{\mu \in A, \nu \in B} \text{Im} \{ H_{\mu\nu}^* (\overline{\mathbf{G}} \Gamma_L \mathbf{G}^\dagger)_{\mu\nu} - H_{\mu\nu}^* (\overline{\mathbf{G}} \Gamma_R \mathbf{G}^\dagger)_{\mu\nu} \}, \quad (3)$$

where \vec{u}_{AB} is the unit vector in the direction from A to B, and μ and ν are related to the atomic orbital indices. Using the first-principles NEGF-DFT, we can estimate \vec{J}_A of Eq. (3) strictly.⁸² More details on NEGF can be found in the literature.⁸³⁻⁸⁵

The structure of contact is the periodic molecular model, just as given in Sec. III. We first report the transport properties of 1L and 2L contacts, and then we analyze the 3L contact in detail, also predicting the transport properties for further stacking.

B. Results of Ag electrodes

Figure 4 shows results of transport properties of Ag(111)/PTCDA/Ag(111) (transmission coefficient; density of states (DOS), of PMOs; and I - V curve and electron pathway) for 1L (a), 2L (b), and 3L (c) contacts. Roughly, the energy level of each PMO relates to the peak of spectrum of the transmission coefficient and $\psi_{\text{LUMO}}^{n(mL)}$ has a large DOS around the Fermi level, dominating electron transport. While $\psi_{\text{LUMO}+1}^{1(1L)}$ has a finite DOS at the Fermi level, $\psi_{\text{LUMO}+1}^{1(2L,3L)}$ shifts from the Fermi level because of the interfacial dipole increase. This is also clear from the electron pathway, because the long edges of PTCDA molecules have large vectors. It has been reported that $\psi_{\text{LUMO}}^{1(1L)}$ has a large amplitude around H atoms while $\psi_{\text{LUMO}+1}^{1(1L)}$ has a large amplitude at the center of the PTCDA molecule.²⁶ In the 1L contact, the vector from the Ag electrode to the center of the PTCDA molecule indicates that the Shockley-type interfacial state, $\psi_{\text{LUMO}+1}^{1(1L)}$, facilitates the charge injection from the substrate. However, this vector disappears because of the shift of $\psi_{\text{LUMO}+1}$ when the number of PTCDA layers is more than two. The electron pathway also shows that the electron mainly displaces in the π stacking direction and not laterally, even for the 3L contact.

In addition, the coupling parameters indicate the differences in the interactions of PMOs, with electrodes between ψ_{LUMO} and $\psi_{\text{LUMO}+1}$ of the 1L contact, i.e., $\gamma(\psi_{\text{LUMO}}^{1(1L)})$ and $\gamma(\psi_{\text{LUMO}+1}^{1(1L)})$. As a consequence of the moderate coupling with the electrode state, $\psi_{\text{LUMO}}^{1(1L)}$ broadens ($\gamma(\psi_{\text{LUMO}}^{1(1L)})$ is 0.60 eV). However, a very small value of $\gamma(\psi_{\text{LUMO}+1}^{1(1L)})$, 0.09 eV, and a sharp peak of DOS show that $\psi_{\text{LUMO}+1}^{1(1L)}$ couples weakly with the electrodes. This is consistent with $\psi_{\text{LUMO}+1}^{1(1L)}$ being part of the Shockley-type interfacial state of Ag(111) and dispersing strongly in a direction parallel to the surface. The values of $\gamma(\psi_{\text{LUMO/LUMO}+1}^{1(2L,3L)})$ are reduced to around 1/3 when the number of PTCDA layers are increased, but a similar description is satisfied. The effect of very low $\gamma(\psi_{\text{LUMO}+1}^{1(1L)})$ can be seen in the resulting I - V curves shown in Figs. 4(a) and 4(b), which contain a few slopes. These slopes are formed by sharp transmission peaks derived from $\psi_{\text{LUMO}+1}^{1(1L)}$.

In the 3L contact, the peak of DOS of PMOs splits according to whether the associating PTCDA touches the electrodes directly. The peaks of PMOs of both edge PTCDA molecules have almost the same features as those of the 1L and 2L contacts, i.e., broadened $\psi_{\text{LUMO}}^{1,3(3L)}$ and sharpened $\psi_{\text{LUMO}+1}^{1,3(3L)}$. However, because of the reduction in the coupling parameters ($\Delta(\psi_{\text{LUMO}}^{2(3L)})$ and $\Delta(\psi_{\text{LUMO}}^{1,3(3L)})$ are 0.22 and 0.09 eV, respectively), $\psi_{\text{LUMO}}^{2(3L)}$ splits from $\psi_{\text{LUMO}}^{1,3(3L)}$. In addition, a striking reduction in $\gamma(\psi_{\text{LUMO}}^{2(3L)})$ of 0.11 eV, which is smaller than $\gamma(\psi_{\text{LUMO}}^{1(1L)}) = 0.60$ or $\gamma(\psi_{\text{LUMO}}^{1(3L)}) = 0.23$, induces a very sharp peak of $\psi_{\text{LUMO}}^{2(3L)}$. This is a fingerprint of a screened PTCDA-Ag interaction

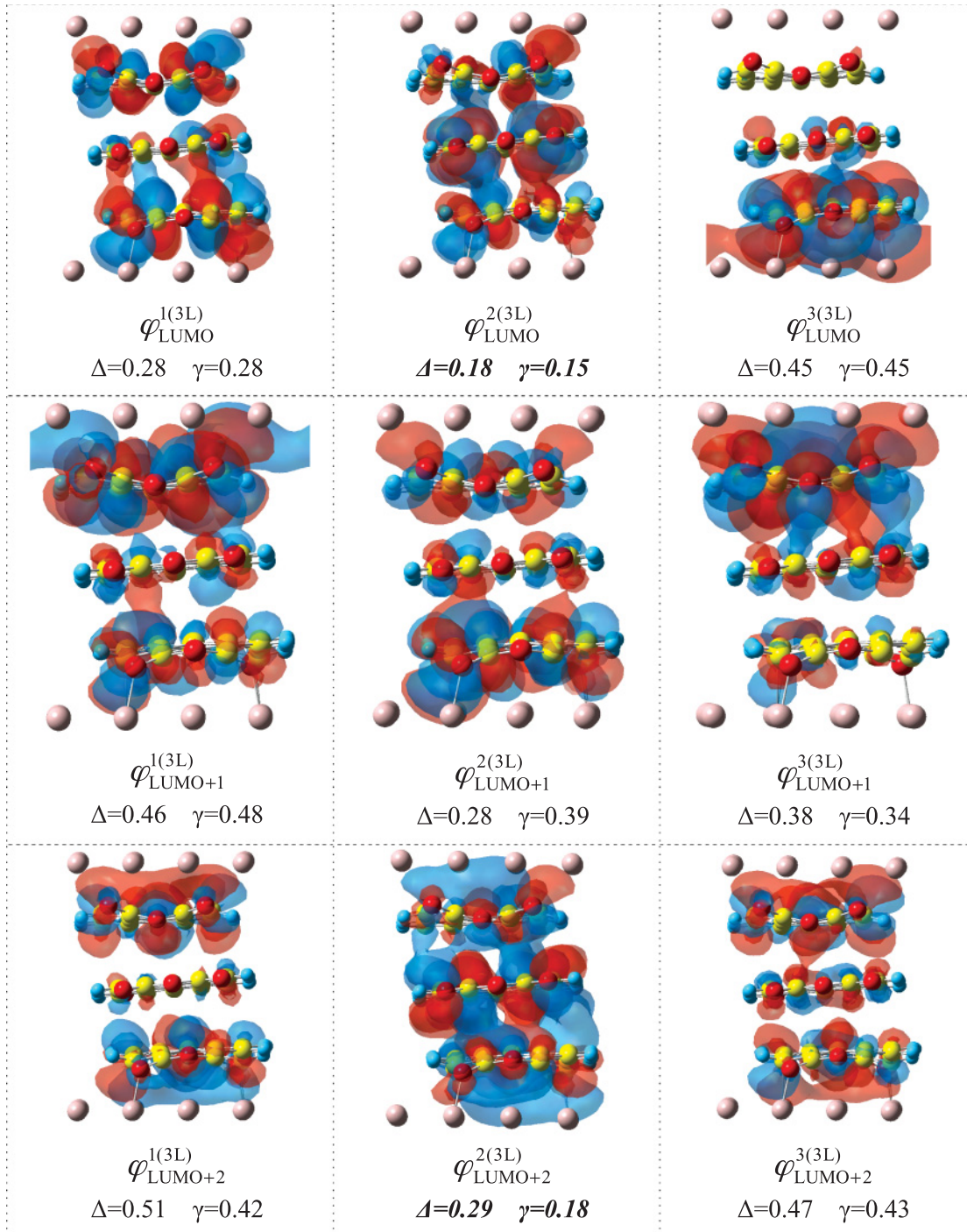


FIG. 6. (Color online) Spatial distributions of PMOs of the 3L contact of Al(111)/PTCDA/Al(111). The numerical values under the labels of PMOs are coupling parameters, and $\Delta(\varphi_{\alpha}^{n(3\text{L})})$ and $\gamma(\varphi_{\alpha}^{n(3\text{L})})$ are calculated by expanding self-energy operators using the wave function of whole molecules. The coupling parameters of conductive orbitals are indicated in bold-italic font.

and supported by an experimental measurement of the fast screening effect by the surface Raman experiment.⁴⁸ The stacked PTCDA layers do not “feel” PTCDA-Ag interactions, and vibrational frequencies converge to those of the PTCDA crystal by stacking more than three PTCDA layers. This fast screening of the PTCDA-Ag interaction partly results from the d -electron screening at the Ag(111) surface, which typically reduces the coupling between the adsorbate and the

substrate and increases the lifetime of the surface state.^{86–88} On the other hand, while $\psi_{\text{LUMO}+1}^{2(3\text{L})}$ shows splitting from $\psi_{\text{LUMO}+1}^{1,3(3\text{L})}$ by reduction in $\Delta(\psi_{\text{LUMO}+1}^{2(3\text{L})})$, the peak remained sharp, because initially $\gamma(\psi_{\text{LUMO}+1})$ is close to zero. As a result, electrons pass through $\psi_{\text{LUMO}}^{2(3\text{L})}$ and $\psi_{\text{LUMO}+1}^{1,2,3(3\text{L})}$ via resonant tunneling, which gives very sharp transmission peaks and, consequently, steplike I - V curves, as shown in Fig. 4(c). Furthermore, because the coupling parameters are already

close to zero, additional stacking of PTCDA would not induce further splitting of DOS of PMOs. Therefore, the I - V curve is expected to keep its shape even by increasing thickness of PTCDA layers. It is noticeable that the Shockley-type state does not contribute to transport directly in the 2L and 3L contacts (this is also clear in the view of the electron pathway) but rather participates in determining the whole shape of the transmission coefficient and hence the I - V curve, even in the higher thickness region.

C. Results of Al electrodes

The Al electrodes were examined using the same approach as used for the Ag case. Figure 5 shows the transmission coefficient, DOS of PMOs, and I - V curves of Al(111)/PTCDA/Al(111) contacts. In the 1L and 2L contacts, $\psi_{\text{LUMO}+1}^{1(1,2L)}$ are broadened remarkably by coupling with the bulk states of Al. This result is supported by an analysis of surface-slab model, PTCDA/Al(111), where the Shockley-type interfacial state is not formed (see Sec. II and references therein). Other PMOs also have large coupling parameters, indicating strong chemical bonding between PTCDA and Al(111) surfaces. For example, $\gamma(\psi_{\text{LUMO}}^{1(1L)})$ and $\gamma(\psi_{\text{LUMO}+1}^{1(1L)})$ are 0.55 and 0.69 eV, respectively, and they do not decrease even in the 2L and 3L contacts. Therefore, these PMOs largely overlap each other and then cause the broad transmission coefficient and completely ohmic I - V characteristics, as shown in Figs. 5(a) and 5(b).

In the 3L contact, the transmission coefficient is characterized by a few sudden sharp peaks, although these are still broader than those seen in the Ag case. Comparison between (b) and (c) of Fig. 5 indicates that these sharp peaks correspond to the PMOs associated with PTCDA in the middle layer. Other peaks do not seem to contribute to transport—contrary to the Ag case, in which all PMOs contribute to the transmission.

Knowledge of coupling *between molecules* is a fundamental prerequisite to understanding the mechanism of the possible contribution of restricted PMOs to transport in the 3L contact. To accomplish this mandatory requirement, we introduce another set of PMOs in which the projection is defined on *entire* PTCDA layers. We denote these PMOs as $\varphi_{\alpha}^{n(3L)}$, where 3L represents the 3L contact just as in $\psi_{\alpha}^{n(3L)}$. The index n indicates that $\varphi_{\alpha}^{n(3L)}$ has a large amplitude on the n th layer of PTCDA. (Specifying n is done for convenience; e.g., $\varphi_{\text{LUMO}+2}^{1(3L)}$ and $\varphi_{\text{LUMO}+2}^{3(3L)}$ are not strictly distinguishable because of the symmetric conformation of first and third layers.) The orbital label α no longer belongs to a single PTCDA because of the definition, and we label it from the energy level. The plots of wave functions of PMOs as $\varphi_{\alpha}^{n(3L)}$ and their coupling parameters are shown in Fig. 6. Here, $\varphi_{\text{LUMO}}^{1,3(3L)}$ are localized around the interface and do not continue to the opposite surface of electrodes because of the large $\gamma(\varphi_{\text{LUMO}}^{1,3(3L)})$; i.e., while $\varphi_{\text{LUMO}}^{1,3(3L)}$ strongly coupled with the electrode states, they were no longer associated with the original MOs of the PTCDA molecule. On the other hand, $\varphi_{\text{LUMO}+2}^{2(3L)}$, whose couplings with the electrode states were slightly weakened, are unevenly distributed to the whole molecules. The relationship between $\varphi_{\text{LUMO}+2}^{1,3(3L)}$ and $\varphi_{\text{LUMO}+2}^{2(3L)}$ is the same as that between $\varphi_{\text{LUMO}}^{1,3(3L)}$ and $\varphi_{\text{LUMO}}^{2(3L)}$.

Because of the localization, $\varphi_{\text{LUMO}+1}^{1,2,3(3L)}$ do not contribute to transport.

We can see from Fig. 6 that $\varphi_{\text{LUMO}}^{2(3L)}$ and $\varphi_{\text{LUMO}+2}^{2(3L)}$ still have larger values of γ because of strong coupling between the PTCDA molecule and the Al electrode. This means that PTCDA-Al interactions were not screened sufficiently by three PTCDA layers. Although the I - V characteristics of the 3L contact of Al(111)/PTCDA/Al(111) shown in Fig. 5(c) show a few slopes, the gradient of each slope is much steeper and shows more ohmic behavior than those of Ag(111)/PTCDA/Ag(111) (Fig. 4(c)). However, further stacking of PTCDA layers produces sharper transmission and a more steplike I - V curve, as in the Ag case. This is because PMOs strongly coupled with electrodes do not contribute to transport, sharpening the threshold of the I - V curve. This consequent Schottky behavior (exponential I - V) is well documented experimentally.⁶⁴

V. CONCLUSION

We calculated the electronic structures and transport properties of PTCDA contact for Ag(111) and Al(111) electrodes using NEGF-DFT and evaluated the roles that intrinsic properties of the metal surfaces play in the transport properties at the interfaces. We adopted periodic molecular structures, which have nonnegligible lateral interactions, and applied NEGF-DFT calculations to up to three stacked PTCDA layers. The periodic molecular structure is a good approximation of (experimentally observed) commensurate layer structure. We revealed that LUMO and LUMO+1 mainly contribute to transport in both systems and the formation of a strong O-Al bond in the case of Al. Because of the existence of the Shockley state and the fast screening of molecule-metal interaction, the coupling parameters of PMOs are small in the Ag case and large in the Al case, producing a relatively ohmic I - V curve of the Al/PTCDA/Al contact.

Even more strikingly, with the aid of the quantitative evaluation of the coupling parameters and electron pathway, we found that the Shockley-type interfacial state at the interface of the PTCDA and Ag(111) surface affected the whole shape of the transmission spectrum and the I - V curve through interactions between states associated with PTCDA layers. Therefore, the microscopic aspect of unique interfacial states was crucial for the transport properties, as well as the macroscopic interfacial dipole. Therefore, precise understanding of transport properties from first-principles calculations is important. The present Ag(111)/PTCDA/Ag(111) contact shows tunneling through well-separated MOs in three layers.

We predicted the I - V characteristics of both systems with thicker molecular layers and showed Schottky behavior through the further stacking of PTCDA. In the case of the Ag electrode, this is because of the Shockley-type interfacial state and the reduction of the PTCDA-Ag interaction. On the other hand, a steplike I - V curve is predicted for the Al electrode, because the only free-molecular-like PTCDA in the middle of the layer contributes to transport; i.e., strongly deformed PMOs at the interface are “hidden” by the PTCDA-Al interaction.

ACKNOWLEDGMENTS

Authors thank G. Giorgi (University of Tokyo) for useful comments. This research was supported by the Global COE Program for Chemistry Innovation through Cooperation of

Science and Engineering from MEXT of Japan, by Grant-in-Aid for Scientific Research on Priority Area No. 2003801 (H.N.) from MEXT of Japan, and by Grants-in-Aid for Scientific Research (C) No. 20613002 (H.N.) and (A) No. 21245004 (K.Y.) from JSPS.

*hs-nakamura@aist.go.jp

- ¹C. W. Tang, *Appl. Phys. Lett.* **48**, 183 (1986).
- ²M. A. Baldo and S. R. Forrest, *Phys. Rev. B* **64**, 085201 (2001).
- ³Y. Shirota and H. Kageyama, *Chem. Rev.* **107**, 953 (2007).
- ⁴T. N. Ng, W. R. Silveira, and J. A. Marohn, *Phys. Rev. Lett.* **98**, 066101 (2007).
- ⁵W. R. Silveira and J. A. Marohn, *Phys. Rev. Lett.* **93**, 116104 (2004).
- ⁶H. Ishii, K. Sugiyama, E. Ito, and K. Seki, *Adv. Mater.* **11**, 972 (1999).
- ⁷S. Kera, Y. Yabuuchi, H. Yamane, H. Setoyama, K. K. Okudaira, A. Kahn, and N. Ueno, *Phys. Rev. B* **70**, 085304 (2004).
- ⁸T. Yokoyama, D. Yoshimura, E. Ito, H. Ishii, Y. Ouchi, and K. Seki, *Jpn. J. Appl. Phys. 1.* **42**, 3666 (2003).
- ⁹D. Wegner, R. Yamachika, Y. Wang, V. W. Brar, B. M. Bartlett, J. R. Long, and M. F. Crommie, *Nano Lett.* **8**, 131 (2008).
- ¹⁰I. G. Hill, A. Rajagopal, A. Kahn, and Y. Hu, *Appl. Phys. Lett.* **73**, 662 (1998).
- ¹¹R. Strohmaier, C. Ludwig, J. Petersen, B. Gompf, and W. Eisenmenger, *Surf. Sci.* **351**, 292 (1996).
- ¹²A. Bannani, C. Bobisch, and R. Moller, *Science* **315**, 1824 (2007).
- ¹³A. Alkauskas, A. Baratoff, and C. Bruder, *Phys. Rev. B* **73**, 165408 (2006).
- ¹⁴Y. Morikawa, T. Hayashi, C. C. Liew, and H. Nozoye, *Surf. Sci.* **507**, 46 (2002).
- ¹⁵Y. Morikawa, C. C. Liew, and H. Nozoye, *Surf. Sci.* **514**, 389 (2002).
- ¹⁶K. Shinoda, W. Shinoda, C. C. Liew, S. Tszuzuki, Y. Morikawa, and M. Mikami, *Surf. Sci.* **556**, 109 (2004).
- ¹⁷K. Takeuchi, S. Yanagisawa, and Y. Morikawa, *Sci. Technol. Adv. Mat.* **8**, 191 (2007).
- ¹⁸S. Bedwani, D. Wegner, M. F. Crommie, and A. Rochefort, *Phys. Rev. Lett.* **101**, 216105 (2008).
- ¹⁹J. P. Jalkanen and F. Zerbetto, *J. Phys. Chem. B* **110**, 5595 (2006).
- ²⁰D. Lamoen, P. Ballone, and M. Parrinello, *Phys. Rev. B* **54**, 5097 (1996).
- ²¹H. Vazquez, R. Oszwaldowski, P. Pou, J. Ortega, R. Perez, F. Flores, and A. Kahn, *Europhys. Lett.* **65**, 802 (2004).
- ²²Y. Morikawa, H. Ishii, and K. Seki, *Phys. Rev. B* **69**, 041403 (2004).
- ²³S. Yanagisawa and Y. Morikawa, *Jpn. J. Appl. Phys.* **45**, 413 (2006).
- ²⁴S. Yanagisawa and Y. Morikawa, *Chem. Phys. Lett.* **420**, 523 (2006).
- ²⁵R. I. R. Blyth, F. Mittendorfer, J. Hafner, S. A. Sardar, R. Duschek, F. P. Netzer, and M. G. Ramsey, *J. Chem. Phys.* **114**, 935 (2001).
- ²⁶F. S. Tautz, *Prog. Surf. Sci.* **82**, 479 (2007).
- ²⁷S. Soubatch, R. Temirov, and F. S. Tautz, *Phys. Status Solidi A* **205**, 511 (2008).
- ²⁸F. Pump, R. Temirov, O. Neucheva, S. Soubatch, S. Tautz, M. Rohlfling, and G. Cuniberti, *Appl. Phys. A-Mater.* **93**, 335 (2008).
- ²⁹D. Braun, A. Schirmeisen, and H. Fuchs, *Surf. Sci.* **575**, 3 (2005).
- ³⁰F. S. Tautz, S. Sloboshanin, J. A. Schaefer, R. Scholz, V. Shklover, M. Sokolowski, and E. Umbach, *Phys. Rev. B* **61**, 16933 (2000).
- ³¹M. Bohringer, W. D. Schneider, K. Glockler, E. Umbach, and R. Berndt, *Surf. Sci.* **419**, L95 (1998).
- ³²C. Seidel, C. Awater, X. D. Liu, R. Ellerbrake, and H. Fuchs, *Surf. Sci.* **371**, 123 (1997).
- ³³T. Schmitz-Hubsch, T. Fritz, R. Staub, A. Back, N. R. Armstrong, and K. Leo, *Surf. Sci.* **437**, 163 (1999).
- ³⁴M. Toerker, T. Fritz, H. Proehl, F. Sellam, and K. Leo, *Surf. Sci.* **491**, 255 (2001).
- ³⁵S. Mannsfeld, H. Relchhard, and T. Fritz, *Surf. Sci.* **525**, 215 (2003).
- ³⁶J. Ikonornov, O. Bauer, and M. Sokolowski, *Surf. Sci.* **602**, 2061 (2008).
- ³⁷P. E. Burrows and S. R. Forrest, *Appl. Phys. Lett.* **62**, 3102 (1993).
- ³⁸A. J. Lovinger, S. R. Forrest, M. L. Kaplan, P. H. Schmidt, and T. Venkatesan, *J Appl. Phys.* **55**, 476 (1984).
- ³⁹A. Kraft, R. Temirov, S. K. M. Henze, S. Soubatch, M. Rohlfling, and F. S. Tautz, *Phys. Rev. B* **74**, 041402 (2006).
- ⁴⁰S. Duhm, A. Gerlach, I. Salzmann, B. Broker, R. L. Johnson, F. Schreiber, and N. Koch, *Org. Electron.* **9**, 111 (2008).
- ⁴¹S. K. M. Henze, O. Bauer, T. L. Lee, M. Sokolowski, and F. S. Tautz, *Surf. Sci.* **601**, 1566 (2007).
- ⁴²B. Krause, A. C. Durr, K. Ritley, F. Schreiber, H. Dosch, and D. Smilgies, *Phys. Rev. B* **66**, 235404 (2002).
- ⁴³T. Wagner, A. Bannani, C. Bobisch, H. Karacuban, M. Stohr, M. Gabriel, and R. Moller, *Org. Electron.* **5**, 35 (2004).
- ⁴⁴M. Schneider, E. Umbach, and M. Sokolowski, *Chem. Phys.* **325**, 185 (2006).
- ⁴⁵L. Kilian, E. Umbach, and M. Sokolowski, *Surf. Sci.* **573**, 359 (2004).
- ⁴⁶K. Glockler, C. Seidel, A. Soukopp, M. Sokolowski, E. Umbach, M. Bohringer, R. Berndt, and W. D. Schneider, *Surf. Sci.* **405**, 1 (1998).
- ⁴⁷V. Shklover, F. S. Tautz, R. Scholz, S. Sloboshanin, M. Sokolowski, J. A. Schaefer, and E. Umbach, *Surf. Sci.* **454**, 60 (2000).
- ⁴⁸V. Wagner, T. Muck, J. Geurts, M. Schneider, and E. Umbach, *Appl. Surf. Sci.* **212**, 520 (2003).
- ⁴⁹M. Eremtchenko, J. A. Schaefer, and F. S. Tautz, *Nature* **425**, 602 (2003).
- ⁵⁰R. Temirov, S. Soubatch, A. Luican, and F. S. Tautz, *Nature* **444**, 350 (2006).
- ⁵¹A. Yang, S. T. Shipman, S. Garrett-Roe, J. Johns, M. Strader, P. Szymanski, E. Muller, and C. Harris, *J. Phys. Chem. C* **112**, 2506 (2008).
- ⁵²A. Hauschild, K. Karki, B. C. C. Cowie, M. Rohlfling, F. S. Tautz, and M. Sokolowski, *Phys. Rev. Lett.* **94**, 036106 (2005).
- ⁵³A. Hauschild, K. Karki, B. C. C. Cowie, M. Rohlfling, F. S. Tautz, and M. Sokolowski, *Phys. Rev. Lett.* **95**, 209602 (2005).
- ⁵⁴R. Rurali, N. Lorente, and P. Ordejon, *Phys. Rev. Lett.* **95**, 209601 (2005).
- ⁵⁵E. Kawabe, H. Yamane, R. Sumii, K. Koizumi, Y. Ouchi, K. Seki, and K. Kanai, *Org. Electron.* **9**, 783 (2008).

- ⁵⁶L. Kilian, A. Hauschild, R. Temirov, S. Soubatch, A. Scholl, A. Bendounan, F. Reinert, T. L. Lee, F. S. Tautz, M. Sokolowski, and E. Umbach, *Phys. Rev. Lett.* **100**, 136103 (2008).
- ⁵⁷Y. Zou, L. Kilian, A. Scholl, T. Schmidt, R. Fink, and E. Umbach, *Surf. Sci.* **600**, 1240 (2006).
- ⁵⁸L. Romaner, D. Nabok, P. Puschnig, E. Zojer, and C. Ambrosch-Draxl, *New J. Phys.* **11**, 053010 (2009).
- ⁵⁹M. Rohlfing, R. Temirov, and F. S. Tautz, *Phys. Rev. B* **76**, 115421 (2007).
- ⁶⁰C. H. Schwalb, S. Sachs, M. Marks, A. Scholl, F. Reinert, E. Umbach, and U. Hofer, *Phys. Rev. Lett.* **101**, 146801 (2008).
- ⁶¹M. Heinrichsmeier, A. Fleszar, and A. G. Eguiluz, *Surf. Sci.* **285**, 129 (1993).
- ⁶²M. Heinrichsmeier, A. Fleszar, W. Hanke, and A. G. Eguiluz, *Phys. Rev. B* **57**, 14974 (1998).
- ⁶³Y. Hirose, A. Kahn, V. Aristov, P. Soukiassian, V. Bulovic, and S. R. Forrest, *Phys. Rev. B* **54**, 13748 (1996).
- ⁶⁴R. Agrawal and S. Ghosh, *Appl. Phys. Lett.* **89**, 222114 (2006).
- ⁶⁵P. Hohenberg and W. Kohn, *Phys. Rev. A* **140**, 1133 (1965).
- ⁶⁶J. M. Soler, E. Artacho, J. D. Gale, A. Garcia, J. Junquera, P. Ordejon, and D. Sanchez-Portal, *J. Phys. Condens. Matter* **14**, 2745 (2002).
- ⁶⁷N. Troullier and J. L. Martins, *Phys. Rev. B* **43**, 8861 (1991).
- ⁶⁸L. Kleinman and D. M. Bylander, *Phys. Rev. Lett.* **48**, 1425 (1982).
- ⁶⁹H. J. Monkhorst and J. D. Pack, *Phys. Rev. B* **13**, 5188 (1976).
- ⁷⁰S. Sachs, C. H. Schwalb, M. Marks, A. Scholl, F. Reinert, E. Umbach, and U. Hofer, *J. Chem. Phys.* **131**, 144701 (2009).
- ⁷¹S. Picozzi, A. Pecchia, M. Gheorghe, A. Di Carlo, P. Lugli, B. Delley, and M. Elstner, *Phys. Rev. B* **68**, 195309 (2003).
- ⁷²P. C. Rusu, G. Giovannetti, C. Weijtens, R. Coehoorn, and G. Brocks, *J. Phys. Chem. C* **113**, 9974 (2009).
- ⁷³N. Nicoara, O. Paz, J. Mendez, A. M. Baro, J. M. Soler, and J. M. Gomez-Rodriguez, *Phys. Rev. B* **82**, 075402 (2010).
- ⁷⁴J. P. Perdew, K. Burke, and M. Ernzerhof, *Phys. Rev. Lett.* **77**, 3865 (1996).
- ⁷⁵S. X. Du, H. J. Gao, C. Seidel, L. Tsetseris, W. Ji, H. Kopf, L. F. Chi, H. Fuchs, S. J. Pennycook, and S. T. Pantelides, *Phys. Rev. Lett.* **97**, 156105 (2006).
- ⁷⁶G. Roman-Perez and J. M. Soler, *Phys. Rev. Lett.* **103**, 096102 (2009).
- ⁷⁷M. Dion, H. Rydberg, E. Schroder, D. C. Langreth, and B. I. Lundqvist, *Phys. Rev. Lett.* **82**, 246401 (2004).
- ⁷⁸K. S. Thygesen and A. Rubio, *Phys. Rev. B* **77**, 115333 (2008).
- ⁷⁹D. J. Mowbray, G. Jones, and K. S. Thygesen, *J. Chem. Phys.* **128**, 111103 (2008).
- ⁸⁰J. B. Neaton, M. S. Hybertsen, and S. G. Louie, *Phys. Rev. Lett.* **97**, 216405 (2006).
- ⁸¹K. Stokbro, J. Taylor, M. Brandbyge, J.-L. Mozos, and P. Ordejon, *Comput. Mater. Sci.* **27**, 151 (2003).
- ⁸²A. Cresti, R. Farchioni, G. Grosso, and G. P. Parravicini, *Phys. Rev. B* **68**, 075306 (2003).
- ⁸³H. Nakamura and K. Yamashita, *J. Chem. Phys.* **125**, 194106 (2006).
- ⁸⁴H. Nakamura, K. Yamashita, A. R. Rocha, and S. Sanvito, *Phys. Rev. B* **78**, 235420 (2008).
- ⁸⁵H. Nakamura, *J. Phys. Chem. C* **114**, 12280 (2010).
- ⁸⁶P. M. Echenique, J. M. Pitarke, E. V. Chulkov, and A. Rubio, *Chem. Phys.* **251**, 1 (2000).
- ⁸⁷P. M. Echenique, R. Berndt, E. V. Chulkov, T. H. Fausterd, A. Goldmann, and U. Hofer, *Surf. Sci. Rep.* **52**, 219 (2004).
- ⁸⁸M. Becker, S. Crampin, and R. Berndt, *Phys. Rev. B* **73**, 081402 (2006).